Polymer 55 (2014) 944–950

Contents lists available at ScienceDirect

Polymer

journal homepage: www.elsevier.com/locate/polymer

# Magnetoresistive conductive polymer-tungsten trioxide nanocomposites with ultrahigh sensitivity at low magnetic field

Hongbo Gu [a,b], Jiang Guo [b], Huige Wei [b], Xi Zhang [b,c], Jiahua Zhu [b,d], Lu Shao [a], Yudong Huang [a,**], Neel Haldolaarachchige [e], David P. Young [e], Suying Wei [b,c,*], Zhanhu Guo [b,*]

[a] School of Chemical Engineering and Technology, Harbin Institute of Technology, Harbin 150001, Heilongjiang, China
[b] Integrated Composites Laboratory (ICL), Dan F. Smith Department of Chemical Engineering, Lamar University, Beaumont, TX 77710, USA
[c] Department of Chemistry and Biochemistry, Lamar University, Beaumont, TX 77710, USA
[d] Department of Chemical & Biomolecular Engineering, University of Akron, Akron, OH 44325, USA
[e] Department of Physics and Astronomy, Louisiana State University, Baton Rouge, LA 70803, USA

ARTICLE INFO

*Article history:*
Received 24 October 2013
Received in revised form
1 December 2013
Accepted 12 December 2013
Available online 21 December 2013

*Keywords:*
Non-magnetic conductive polymer nanocomposites
Electron transport
Magnetoresistance

ABSTRACT

The effect of conductive polymer matrix including polyaniline (PANI) and polypyrrole (PPy) on the magnetoresistance (MR) behaviors in the variable range hopping (VRH) regime has been investigated in the disordered polymer nanocomposites containing tungsten trioxide ($WO_3$) nanoparticles. These nanocomposites have demonstrated ultrahigh MR sensitivity at low magnetic field regime. The observed positive MR has been well explained by the wave-function shrinkage model. The conductive polymer matrix has shown different effects on the MR behaviors of the nanocomposites. The $WO_3$/PANI nanocomposites have a lower localization length ($a_0$) and density of states at the Fermi level ($N(E_F)$), and higher average hopping distance ($R_{hop}$) and average hopping energy ($W$) compared with those of the $WO_3$/PPy nanocomposites.



## 1. Introduction

The magnetoresistance (MR) phenomenon, defined as $\Delta R/R = [R(B) - R(0)]/R(0)$, describes the resistance change of a material under an applied external magnetic fields [1]. Since the first discovery of huge MR change, which is called giant magnetoresistance (GMR) effect, in the thin-film structural metallic materials composed of a pair of ferromagnetic layers (Fe) separated by a non-magnetic metal layer (Cr) in 1988 [2,3], GMR-based electronics have been developed and widely used in the areas including rotation speed sensing, angular position sensing, biosensors and biochips, magnetic field sensors, hard disc drivers and magnetic random access memory (MRAM) in computers [4,5]. In the last decade, the GMR effect in conductive polymers and their nanocomposite systems has attracted intense interests due to their easy synthesis, low cost, high conductivity and relatively high GMR signals compared with other organic semiconductors [5,6]. For example, around 95% GMR has been reported in the magnetic *p*-toluene sulfonic acid (PTSA) doped polyaniline (PANI) nanocomposites with a $Fe_3O_4$ nanoparticle loading of 30 wt% synthesized using surface initiated polymerization (SIP) method and 53% GMR in the PTSA doped pure PANI [1]. About 20% of GMR in the non-magnetic PANI nanocomposites with a $BaTiO_3$ (~500 nm) loading of 20 wt% synthesized by SIP method and around 35% GMR in the 20 wt% $BaTiO_3$ (~500 nm)/PANI nanocomposites prepared by simple physical mixture of PANI and $BaTiO_3$ powders have been reported [7]. Later on, up to 95.5% GMR was reported in the phosphoric acid ($H_3PO_4$) doped non-magnetic PANI nanocomposites with 20 wt% silica nanoparticle loading and 65.6 wt% GMR in the $H_3PO_4$ doped pure PANI [8]. Meanwhile, a GMR effect of around 22% in the non-magnetic silicon/PANI nanocomposites was reported [9]. In addition, a room temperature MR transition from positive to negative has been reported in the silicon/PANI nanocomposites with a silicon loading of 10 wt% in the variable range hopping (VRH) regime and the wave-function shrinkage model and forward interference model have been used to separate the positive and negative MR from the obtained MR results [10].

* Corresponding authors. Integrated Composites Laboratory (ICL), Dan F. Smith Department of Chemical Engineering, Lamar University, Beaumont, TX 77710, USA.
** Corresponding author.
*E-mail addresses:* huangyd@hit.edu.cn (Y. Huang), suying.wei@lamar.edu (S. Wei), zhanhu.guo@lamar.edu (Z. Guo).

0032-3861/$ – see front matter © 2013 Elsevier Ltd. All rights reserved.
http://dx.doi.org/10.1016/j.polymer.2013.12.024

Conducting polymers, such as polyacetylene (PA), PANI, polypyrrole (PPy), polythiophenes (PTs) and poly(DNTD), have gained more attentions in the last few decades [11] since the first discovery of the electrical conduction in doped PA [12]. They have been widely used in the applications including electronics [13], fire retardants [14], electrodes for electrodeposition [15] and supercapacitors [16,17]. Tungsten trioxide ($WO_3$), a n-type semiconductor with a band gap of 2.7 eV, has been widely used in electrochromic devices [16], photocatalysts [17], gas sensors [18], fuel cell catalyst support [19], and photochromic process [20] due to its good chemical stability and genuine color switching. PANI and PPy are two most used conducting polymers due to their easy synthesis and doping/dedoping process [21]. Even though the PANI and PPy nanocomposites with $WO_3$ nanoparticles have been synthesized using a surface initiated polymerization (SIP) method [22,23], the MR behaviors of these nanocomposites have not been reported yet so far.

In this paper, the effect of conductive polymer matrix including PANI and PPy on the GMR behaviors of the non-magnetic disordered conductive polymer nanocomposites with different $WO_3$ nanoparticle loading in the disordered VRH regime is investigated. The morphology and crystallization structure of the synthesized $WO_3$/PANI and $WO_3$/PPy nanocomposites are studied. The ultrahigh MR sensitivity at low magnetic field in these nanocomposites is analyzed by the wave-function shrinkage model.

## 2. Experimental

### 2.1. Materials

Aniline ($C_6H_7N$), pyrrole ($C_4H_5N$) and ammonium persulfate (APS, $(NH_4)_2S_2O_8$), and *p*-toluene sulfonic acid (PTSA, $C_7H_8O_3S$) were purchased from Sigma Aldrich. The $WO_3$ nanoparticles (99+%) with an average diameter of 30 nm were obtained from Nanostructured & Amorphous Materials, Inc. All the chemicals were used as-received without any further treatment.

### 2.2. Preparation of $WO_3$/PANI and $WO_3$/PPy nanocomposites

The $WO_3$/PANI and $WO_3$/PPy nanocomposites were fabricated using SIP method. A certain amount of $WO_3$ nanoparticles was mixed in a solution of PTSA and APS with a ratio of 15 mmol: 9 mmol in 100 mL deionized water in an ice-water bath for 1 h sonication combined with mechanical stirring. The aniline or pyrrole solution (18 mmol in 25 mL deionized water with molar ratio of PTSA: APS: aniline = 5: 3: 6) was mixed with the above solution and then sonicated and mechanically stirred for additional 1 h in an ice-water bath for polymerization. The product was vacuum-filtered and washed with deionized water several times to remove any unreacted PTSA and APS. The precipitant was further washed with methanol to remove any possible oligomers. The final product was dried at 50 °C in an oven overnight. The $WO_3$/PANI nanocomposites with a $WO_3$ loading of 10, 20, 40 and 60 wt% and the $WO_3$/PPy nanocomposites with a $WO_3$ loading of 40 and 60 wt% were prepared following the above procedure.

### 2.3. Characterizations

The morphology of the as-received $WO_3$ nanoparticles and synthesized nanocomposites was examined in the field emission scanning electron microscope (SEM, JEOL, JSM-6700F). The morphology and nanoparticle distribution were further obtained in a Philips CM-200 transmission electron microscopy (TEM) with a LaB6 filament. The samples were prepared by drying a drop of nanocomposite powders ethanol suspension on carbon-coated copper TEM grids.

X-ray diffraction (XRD) analysis was carried out with a Bruker AXS D8 Discover diffractometer with GADDS (General Area Detector Diffraction System) operating with a Cu-K$\alpha$ radiation source filtered with a graphite monochromator ($\lambda = 1.5406$ Å).

The resistivity ($\rho$) was measured by a standard four-probe method from 100 to 290 K. The sample was prepared by pressing $WO_3$/PANI and $WO_3$/PPy nanocomposite powders to disc pellet form with a diameter of 25 mm by applying a pressure of 50 MPa in a hydraulic presser and the average thickness was about 1.0 mm. The temperature dependent resistivity was used to determine the electrical conduction mechanism in the $WO_3$/PANI and $WO_3$/PPy nanocomposites. The same sample was used for the dielectric property test by a LCR meter (Agilent, E4980A) equipped with a dielectric test fixture (Agilent, 16451B) at the frequency range of 20 to $2 \times 10^6$ Hz at room temperature under the alternative electric field.

The same sample was also used for MR measurements using a standard four-probe technique by a 9-T Physical Properties Measurement System (PPMS) by Quantum Design at room temperature. The four probes were 0.002 inch diameter platinum wires, which were attached by silver paste to the sample. And the magnetic field was applied perpendicular to the current.

## 3. Results and discussions

### 3.1. Microstructure observations

The SEM and TEM of 10.0 wt% loading of $WO_3$/PANI and $WO_3$/PPy nanocomposites are shown in Fig. 1 and Fig. S1, respectively. The as-received $WO_3$ nanoparticles, Fig. 1(a), exhibit a ball-like structure and the surface is very smooth. However, after coated with PANI and PPy, the nanocomposites show very different morphologies from the as-received nanoparticles. Fig. 1(b&c) shows the SEM images of 10.0 wt% loading of $WO_3$/PANI and $WO_3$/PPy nanocomposites, respectively. The 10.0 wt% loading of $WO_3$/PANI nanocomposites show very rough surface, Fig. 1(b), indicating the polymerization of the aniline on the surface of the $WO_3$ nanoparticles [24]. The 10.0 wt% loading of $WO_3$/PPy nanocomposites exhibit the particulate microstructure as that of the as-received $WO_3$ nanoparticles, Fig. 1(c). It is obvious that the diameters of the 10.0 wt% loading of $WO_3$/PPy nanocomposites are much bigger than that of the as-received $WO_3$ nanoparticles, illustrating the polymerization of the pyrrole on the surface of $WO_3$ nanoparticles. The TEM images in Fig. S1 show the good dispersion of the nanoparticles within the polymer matrix and a uniform coating layer of polymer outside the nanoparticles is observed. FT-IR results of the synthesized $WO_3$/PANI and $WO_3$/PPy nanocomposites are shown in Fig. S2&S3, respectively. The characteristic peaks of PANI and PPy are observed obviously in the FT-IR spectra, which further confirms that the PANI and PPy present on the surface of $WO_3$ nanoparticles.

### 3.2. X-ray diffraction

The crystallization structures of the as-received $WO_3$ nanoparticles and the synthesized $WO_3$/PANI and $WO_3$/PPy nanocomposites are determined by X-ray diffraction (XRD), Fig. 2. The observed strong intensity of the diffraction peaks in the XRD test of all the samples indicates the highly crystallized structure [22]. The diffraction peaks at around $2\theta = 23.1, 23.65, 24.4, 26.6, 28.8, 33.35, 34.2, 41.55, 47.35, 50.0$ and $55.95^\circ$ in the as-received $WO_3$ nanoparticles, Fig. 2(b), correspond to the (0 0 2), (0 2 0), (2 0 0), (1 2 0), (1 1 2), (0 2 2), (2 0 2), (2 0 1), (2 1 1), (2 2 0) and (2 2 2) crystallographic planes of the crystallized $WO_3$ nanoparticles [25]. The broad peak at around 20° in the 10 wt% loading of $WO_3$/PANI nanocomposites is attributed to the crystallographic planes of the

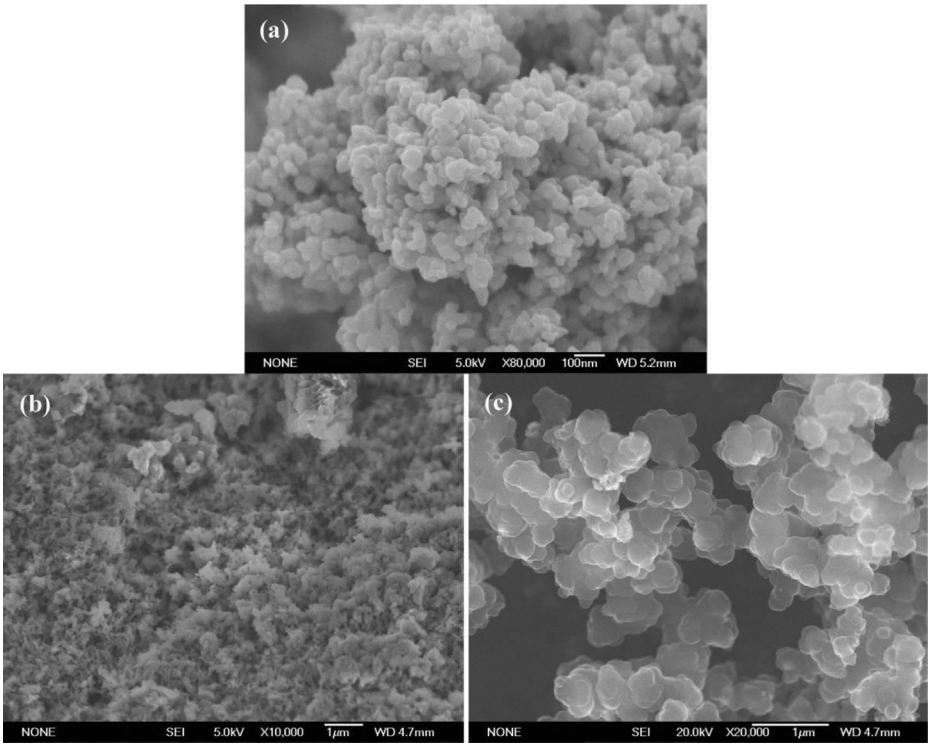


**Fig. 1.** SEM microstructures of (a) as-received $WO_3$ nanoparticles, (b) 10.0 wt% loading of $WO_3$/PANI, and (c) 10 wt% loading of $WO_3$/PPy.

partially crystallized PANI [26] and the intensity of this broad peak decreases and even disappears with increasing the $WO_3$ nanoparticle loading in the $WO_3$/PANI nanocomposites, Fig. 2(a, c, d & e).

The average crystallite size is estimated through XRD pattern using the Scherrer Equation (1) [1]:

$$\beta = \frac{k\lambda}{L\cos\theta} \tag{1}$$

where $\lambda$ is the X-ray wavelength ($\lambda = 0.154$ nm), $L$ is the average crystallite size, $k$ is the shape factor, $\beta$ is the full-width at half-maximum, and $\theta$ is Bragg angle in degree. The shape factor $k$, which depends on several factors including the miller index of the reflection plane and the shape of the crystal, normally is 0.89. The peak at $2\theta = 28.8^\circ$ is chosen to calculate the average crystallite size. The obtained average crystallite size of the $WO_3$ nanoparticles is about 29.4 nm. In the $WO_3$/PANI nanocomposites, the calculated average crystallite size is 25.0, 25.1, 27.0 and 29.5 nm for the $WO_3$/PANI with a $WO_3$ loading of 10, 20, 40 and 60 wt%, respectively. The average crystallite size is 24.9 and 28.7 nm for the $WO_3$/PPy with a $WO_3$ loading of 40 and 60 wt%, respectively. There is little change of the average crystallite size of $WO_3$ nanoparticles after fabrication of the conducting polymer nanocomposites.

### 3.3. Temperature dependent resistivity-electrical conduction mechanism

The temperature dependent resistivity for the $WO_3$/PANI and $WO_3$/PPy nanocomposites is shown in Fig. 3(a&c). The resistivity of all the synthesized samples decreases with increasing temperature, exhibiting a semiconductor behavior from 50 to 290 K [27]. In Fig. 3(a), the resistivity of $WO_3$/PANI nanocomposites obeys the following relationships: 40 wt% $WO_3$/PANI > 60 wt% $WO_3$/PANI > 10 wt% $WO_3$/PANI > 20 wt% $WO_3$/PANI. Higher resistivity is observed in the PANI nanocomposites after the $WO_3$ loading

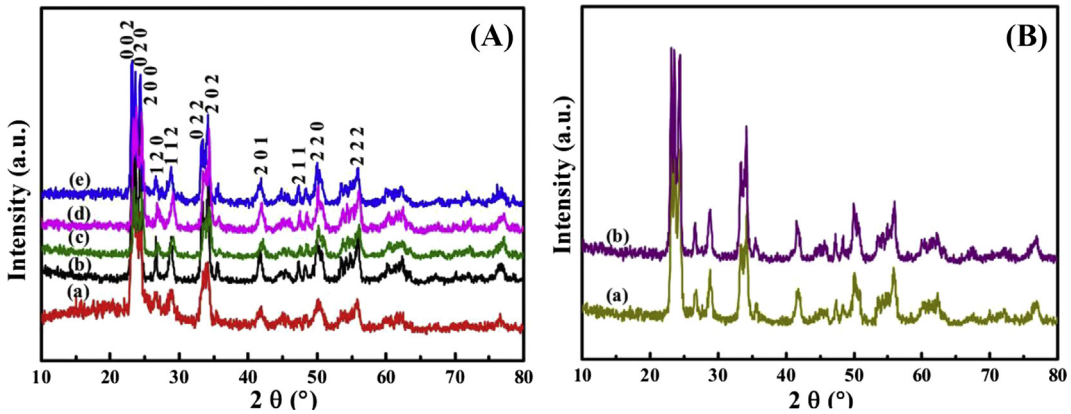


**Fig. 2.** XRD of the (A) $WO_3$/PANI nanocomposites with a $WO_3$ loading of (a) 10, (c) 20, (d) 40, (e) 60 wt% and (b) as-received $WO_3$ nanoparticles; (B) $WO_3$/PANI nanocomposites with a $WO_3$ loading of (a) 40 and (b) 60 wt%.

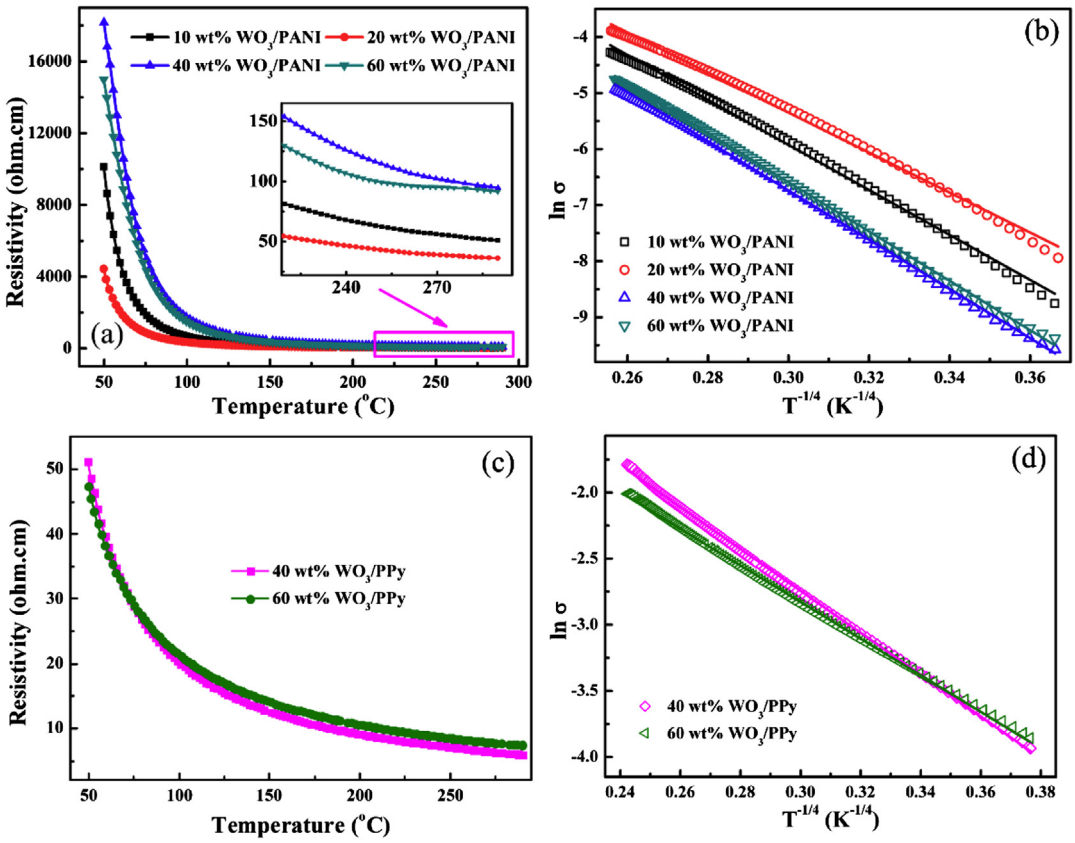


**Fig. 3.** Resistivity *vs.* temperature for the (a) $WO_3$/PANI and (c) $WO_3$/PPy nanocomposites; and ln(σ) and $T^{-1/4}$ curves for (b) $WO_3$/PANI and (d) $WO_3$/PPy nanocomposites.

increases to 40 wt% due to the percolation of the $WO_3$ nanoparticles. Therefore, the resistivity of $WO_3$/PANI with a $WO_3$ nanoparticle loading of 40 and 60 wt% are very close to each other but higher than that of the $WO_3$/PANI nanocomposites with a $WO_3$ nanoparticle loading of 10 and 20 wt%. This is also observed in the $Fe_3O_4$/PANI nanocomposites, in which the resistivity decreases with increasing the nanoparticle loading to 16.67 wt% and increases dramatically as the nanoparticle loading increases to 30 wt% [1]. The resistivity for the $WO_3$/PANI nanocomposites with a $WO_3$ loading of 10, 40 and 60 wt% is decreased by almost 4 orders of magnitude as the temperature increases from 50 to 290 K and the resistivity of the 20 wt% loading of $WO_3$/PANI nanocomposites has 3 orders of magnitude decrease within the temperature range of 50∼290 K. At temperature of 290 K, the highest resistivity of 94.66 Ω.cm is observed in the 40 wt% loading of the $WO_3$/PANI nanocomposites and the lowest resistivity of 36.17 Ω.cm is obtained in the 20 wt% loading of $WO_3$/PANI nanocomposites. In Fig. 3(c), the resistivity of the $WO_3$/PPy nanocomposites with a $WO_3$ loading of 40 and 60 wt% is very similar to each other, which only has a small change from 51.08 to 5.99 Ω.cm for 40 wt% $WO_3$/PPy nanocomposites and from 47.31 to 7.46 Ω.cm for 60 wt% $WO_3$/PPy nanocomposites with the temperature increasing from 50 to 290 K.

The electrical conduction mechanism is investigated through the obtained temperature dependent resistivity using Mott VRH approach, which is expressed as Equation (2) [27]:

$$\sigma = \sigma_0 \exp\left[-\left(\frac{T_0}{T}\right)^{1/n+1}\right] \tag{2}$$

where the constant $\sigma_0$ stands for the conductivity at infinite low temperature, $T$ (K) is the Kelvin temperature, and constant $T_0$(K) is the hopping barrier, which stands for the characteristic Mott temperature and is described as Equation (3) [28]:

$$T_0 = \frac{24}{\pi k_B N(E_F) a_0^3} \tag{3}$$

where $a_0$ is the localization length, $k_B$ is Boltzmann constant and $N(E_F)$ is the density of states at the Fermi level. The value $n$ is the dimension of the system and $n = 3$, 2 and 1 stands for 3-, 2- and 1-dimensional systems, respectively [29]. The $\sigma_0$ and $T_0$ can be obtained from the intercept and slope of the linear fitting $\ln(\sigma) \sim T^{-1/(n+1)}$. In the Mott's VRH mechanism, $T_0$, $a_0$, average hopping distance ($R_{hop}$), and average hopping energy ($W$) are important characteristic parameters. And $R_{hop}$ and $W$ can be expressed as Equations (4) and (5), respectively:

$$R_{hop} = \left(\frac{3}{8}\right)\left(\frac{T_0}{T}\right)^{1/4} a_0 \tag{4}$$

$$W = \frac{3}{4\pi R_{hop}^3 N(E_F)} \tag{5}$$

The best linear fits of $\ln(\sigma) \sim T^{-1/(n+1)}$ for the $WO_3$/PANI and $WO_3$/PPy nanocomposites obtained from Fig. 3(a&c) are shown in Fig. 3(b&d) with $n = 3$ in the temperature range of 50∼290 K, indicating that the synthesized $WO_3$/PANI and $WO_3$/PPy nanocomposites obey quasi 3D VRH hopping mechanism. This means that all the synthesized nanocomposites are disordered system in 3D VRH regime. The calculated $\sigma_0$ and $T_0$ are listed in Table 1. The nanocomposites with the $WO_3$ loading of higher than 40 wt% behave more like a disordered metal than a disordered polymer.

And the conductivity of the 3D disordered metals can be fitted by Equation (6) [30]:

$$\sigma = \sigma_0 + AT^{1/2} + BT^{p/2} \quad (6)$$

where the second term arises from the electron–electron interactions and the third term is related to $\sigma_0$ due to the weak localization effects. In the disordered system, the electron–electron interactions play an important role in the low-temperature electrical transport and the weak localization effects are predominant at the higher temperature. For the 2D disordered system, the conductivity is related to the logarithmic temperature for both the electron–electron interaction and weak localization, which can be expressed as Equation (7) [31,32]:

$$\sigma = \sigma_0 + C \ln T \quad (7)$$

However, the conducting polymer nanocomposites in this work were synthesized by a SIP method and the PANI and PPy have been coated on the surface of nanoparticles. Even for the high loading of $WO_3$ (such as 40 and 60 wt%) in the nanocomposites, the PANI and PPy still can be observed on the surface of $WO_3$ as confirmed from FT-IR analysis in Fig. S2&S3. The conductivity in these systems is dominated by the PANI or PPy phase rather than the metal oxide phase. Therefore, the conductivity is fitted by Mott's law in this work to obtain the important parameter $T_0$.

### 3.4. Room temperature magnetoresistance

The room temperature MR result for the synthesized $WO_3$/PANI and $WO_3$/PPy nanocomposites calculated from MR = (R(*H*) −R(0))/R(0) is shown in Fig. 4(a)&(b), respectively. For the $WO_3$/PANI nanocomposites, Fig. 4(a), the MR shows positive values within the measured magnetic field range and magnetic field (*H*) dependent behaviors. The MR of the $WO_3$/PANI nanocomposites shows the following relationships: 20 wt% $WO_3$/PANI < 10 wt% $WO_3$/PANI < 60 wt% $WO_3$/PANI < 40 wt% $WO_3$/PANI. The MR value of up to 32.63% is observed in the 40 wt% $WO_3$/PANI nanocomposites at an *H* of 7 T. Only 1.65% MR value is obtained for the 20 wt% $WO_3$/PANI nanocomposites at an *H* of 7 T. In Fig. 4(b), the MR of the $WO_3$/PPy nanocomposites also shows positive values in the measured *H* range. At the same loading of $WO_3$ nanoparticles, the MR values of the $WO_3$/PPy nanocomposites are smaller than that of the $WO_3$/PANI nanocomposites at the same *H*, which indicates that the polymer matrix can affect the MR behavior of the nanocomposites. Generally, the magnetic field sensor is based on the MR effect and the MR can be used to present the sensitivity of the materials to the *H* [33]. Thus, the sensitivity of a material to the applied *H* can be expressed as either MR value at the low *H* or linear with respect to the *H* (i.e. slope at low *H*) [34,35]. The slope of the MR curves for the $WO_3$/PANI nanocomposites with a $WO_3$ nanoparticle loading of 10, 20, 40 and 60 wt% is 12.205, 3.434, 163.367 and 134.703 (the corresponding MR value at *H* of 1 T for $WO_3$/PANI nanocomposites with a $WO_3$ nanoparticle loading of 10, 20, 40 and 60 wt% is 1.1, 0.3, 17.12 and 13.80%, respectively), respectively. For the $WO_3$/PPy nanocomposites with a $WO_3$ nanoparticle loading of 40 and 60 wt%, the slope of MR curves is 14.351 and 18.213, respectively. Therefore, the $WO_3$/PANI nanocomposites with a $WO_3$ nanoparticle loading of 40 wt% have the highest sensitivity to the magnetic field and 20 wt% loading of $WO_3$/PANI nanocomposites have the lowest sensitivity to the magnetic field. The room temperature MR results of pure PANI and pure PPy were reported in our previous papers [1,28] and they are shown in Fig. S4. From Fig. S4, the MR of pure PANI and PPy is observed to be very different. Pure PANI has very high MR value of 53% at a magnetic field of 9 T and pure PPy has a lower MR value around 0.4% at a magnetic field of 9 T. This also indicates the polymer matrix effect on the MR property.

**Table 1**
$T_0$ and $\sigma_0$ for the $WO_3$/PANI and $WO_3$/PPy nanocomposites.

| Samples | $T_0$ (K) | $\sigma_0$ (S cm$^{-1}$) |
|---|---|---|
| *$WO_3$/PANI nanocomposites* | | |
| 10 wt% | $2.60 \times 10^6$ | 456.04 |
| 20 wt% | $1.62 \times 10^6$ | 212.55 |
| 40 wt% | $3.72 \times 10^6$ | 622.78 |
| 60 wt% | $3.75 \times 10^6$ | 744.91 |
| *$WO_3$/PPy nanocomposites* | | |
| 40 wt% | $6.29 \times 10^4$ | 7.45 |
| 60 wt% | $3.67 \times 10^4$ | 3.76 |

Generally, for the highly disorderedly localized systems in the VRH regime, the wave-function shrinkage model is often introduced to illustrate the observed positive MR effect [10]. In the wave-function shrinkage model, the common idea is based on the contraction of the electronic wave function at impurity centers in the magnetic field, leading to a reduction in the hopping probability between two sites and causing a positive MR. The $r_{wave}$=$R(H,T)$/$R(0,T)$ is described as Equation (8) [10]:

$$r_{wave} = \exp\{\xi_C(0)[\xi_C(H)/\xi_C(0) - 1]\} \quad (8)$$

where $\xi_C(0)=(T_0/T)^{1/4}$ for the 3D Mott VRH mechanism, $\xi_C(H)$ is the optimum hopping probability parameter, $\xi_C(H)/\xi_C(0)$ is the normalized hopping probability parameter and as a function of $H/P_C$ for Mott VRH mechanism, $P_C$ is the fitting parameter given by Equation (9):

$$P_c = 6\hbar/\left[ea_0^2\xi_C(0)\right] \quad (9)$$

where $e$ is electron charge, $a_0$ is the localization length, $\hbar$ is reduced Planck's constant and $T_0$ is Mott characteristic temperature. In the low-field limit (<1 T), the $r_{wave}$ can be expressed as Equation (10):

$$r_{wave} \approx 1 + t_2\frac{H^2}{P_C^2}\left(\frac{T_0}{T}\right)^{1/4} \quad (10)$$

i.e. Equation (11):

$$\mathrm{MR} = \frac{\Delta R(H,T)}{R(0,T)} \approx t_2\frac{H^2}{P_C^2}\left(\frac{T_0}{T}\right)^{1/4} = t_2\frac{e^2a_0^4}{36\hbar^2}\left(\frac{T_0}{T}\right)^{3/4}H^2 \quad (11)$$

where the numerical constant $t_2 \approx 5/2016$ [36]. In Fig. 4(a), the MR of all the synthesized nanocomposites is observed to sharply increase with increasing *H* for *H* increasing to 0.1 T and then shows the quadratic $H^2$ dependent property. In the wave-function shrinkage model, this magnetic field dependent behavior has been explained as follows: in the low magnetic field, the applied *H* decreased the overlap probability between two sites, resulting in an increased resistance with an increased *H* [34]; in the higher magnetic field, the variable range hopping between the localized states having a Coulomb gap in the density of states at the Fermi level, which causes the quadratic *H* dependent behavior [35].

Thus, the $a_0$ can be calculated from $T_0$, MR and *H* from following Equation (12):

$$a_0^4 = \frac{36\hbar^2 MR}{t_2e^2}\left(\frac{T_0}{T}\right)^{-3/4}H^{-2} \quad (12)$$

For example, the obtained $a_0$ for the 10 wt% $WO_3$/PANI nanocomposites at 290 K is 61.2, 30.8, and 24.4 nm for *H* at 1.0, 5.0, and 9.0 T, respectively. The calculated $a_0$ for the $WO_3$/PANI and $WO_3$/

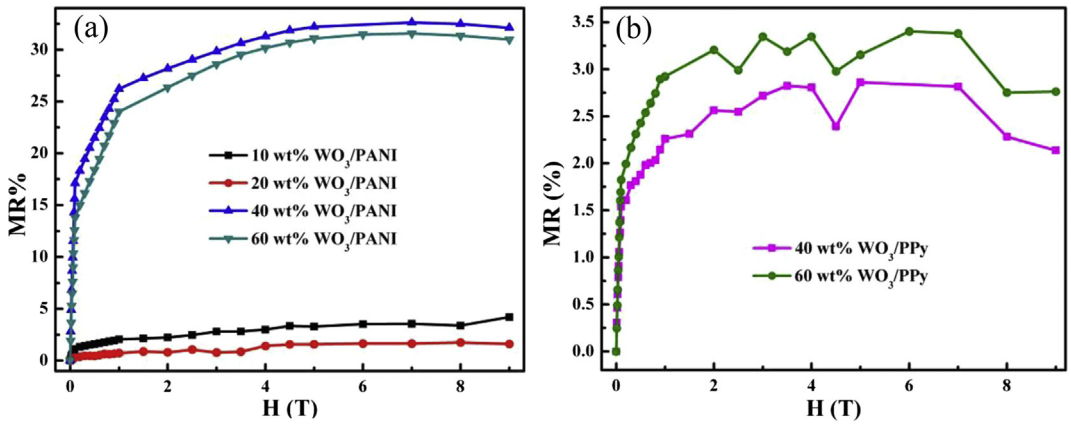


**Fig. 4.** Room temperature magnetoresistance (a) $WO_3$/PANI and (b) $WO_3$/PPy.nanocomposites.

PPy nanocomposites at different $H$ is listed in Table 2. From the calculated results, the $a_0$ is observed to have $H$ dependent property after applying an external $H$ and decreases with increasing $H$. After obtaining $a_0$, the $N(E_F)$ can be calculated from Equation (13) [37]:

$$N(E_F) = \frac{24}{\pi k_B T_0 a_0^3} \tag{13}$$

The calculated corresponding $N(E_F)$ is also listed in Table 2 and the $N(E_F)$ has a $H$ dependent behavior and increases with increasing $H$. The calculated average hopping length $R_{hop}$ and average hopping energy $W$ for the $WO_3$/PANI and $WO_3$/PPy nanocomposites are shown in Table 2, respectively. The calculated $R_{hop}$ (nm) has the $H$ dependent behavior and decreases with increasing $H$. Generally, the positive MR in the hopping system is due to the charge carrier hopping conduction arising from the contraction of the charge carrier wave function and the subsequent reduced $R_{hop}$ [27]. This phenomenon is also observed in the silica/PANI [8], silicon/PANI [9] and $Fe_3O_4$/PPy nanocomposites [28]. The calculated $W$ is observed to be $H$ independent and has no change with increasing $H$. Meanwhile, from Tables 1 and 2, it can be obtained that different polymer matrix with the same $WO_3$ nanoparticle loadings has different Mott parameters including $T_0$, $R_{hop}$ and $W$, and the $WO_3$/PANI nanocomposites have a lower $a_0$ and $N(E_F)$, and higher $R_{hop}$ and $W$ compared with those of the $WO_3$/PPy nanocomposites.

**Table 2**
$a_0$, $N(E_F)$, $R_{hop}$ and $W$ for the $WO_3$/PANI and $WO_3$/PPy nanocomposites at different magnetic field $H$.

| Samples | Parameters | Magnetic field $H$ (T) | | |
|---|---|---|---|---|
| | | 1.0 | 5.0 | 9.0 |
| *$WO_3$/PANI* | | | | |
| 10 wt% | $a_0$ (nm) | 61.2 | 30.8 | 24.4 |
| | $N(E_F)$ (eV cm$^3$)$^{-1}$ | $1.49 \times 10^{14}$ | $1.17 \times 10^{15}$ | $2.35 \times 10^{15}$ |
| | $R_{hop}$ (nm) | 223.3 | 112.4 | 89.0 |
| | $W$ (meV) | 144.1 | 144.1 | 144.1 |
| 20 wt% | $a_0$ (nm) | 51.4 | 27.9 | 21.0 |
| | $N(E_F)$ (eV cm$^3$)$^{-1}$ | $4.02 \times 10^{14}$ | $2.50 \times 10^{15}$ | $5.93 \times 10^{15}$ |
| | $R_{hop}$ (nm) | 166.7 | 90.6 | 68.0 |
| | $W$ (meV) | 128.1 | 128.1 | 128.1 |
| 40 wt% | $a_0$ (nm) | 108.1 | 50.9 | 37.9 |
| | $N(E_F)$ (eV cm$^3$)$^{-1}$ | $1.88 \times 10^{13}$ | $1.80 \times 10^{14}$ | $4.36 \times 10^{14}$ |
| | $R_{hop}$ (nm) | 431.7 | 203.2 | 151.4 |
| | $W$ (meV) | 157.8 | 157.8 | 157.8 |
| 60 wt% | $a_0$ (nm) | 105.7 | 50.4 | 37.5 |
| | $N(E_F)$ (eV cm$^3$)$^{-1}$ | $2.00 \times 10^{13}$ | $1.84 \times 10^{14}$ | $4.36 \times 10^{14}$ |
| | $R_{hop}$ (nm) | 422.6 | 201.5 | 150.9 |
| | $W$ (meV) | 158.2 | 158.2 | 158.2 |
| *$WO_3$/PPy* | | | | |
| 40 wt% | $a_0$ (nm) | 125.8 | 59.7 | 41.4 |
| | $N(E_F)$ (eV cm$^3$)$^{-1}$ | $7.08 \times 10^{14}$ | $6.63 \times 10^{15}$ | $1.99 \times 10^{16}$ |
| | $R_{hop}$ (nm) | 181.1 | 85.9 | 59.5 |
| | $W$ (meV) | 56.8 | 56.8 | 56.8 |
| 60 wt% | $a_0$ (nm) | 148.6 | 67.7 | 48.9 |
| | $N(E_F)$ (eV cm$^3$)$^{-1}$ | $7.37 \times 10^{14}$ | $7.78 \times 10^{15}$ | $2.08 \times 10^{16}$ |
| | $R_{hop}$ (nm) | 186.9 | 85.2 | 61.4 |
| | $W$ (meV) | 49.6 | 49.6 | 49.6 |

## 4. Conclusion

In summary, the $WO_3$/PANI and $WO_3$/PPy nanocomposites exhibit different crystallinity at the same $WO_3$ nanoparticle loading. The conductive disordered $WO_3$/PANI and $WO_3$/PPy nanocomposites have been demonstrated to follow 3-$d$ variable range hopping mechanism by the temperature dependent resistivity study. The observed positive MR is interpreted by the wave-function shrinkage model and well explained by the introduced $a_0$, $N(E_F)$ and $R_{hop}$. The conductive polymer matrices have shown different effects on the MR behaviors of the nanocomposites and the $WO_3$/PANI nanocomposites have an lower $a_0$ and $N(E_F)$, and higher $R_{hop}$ and $W$ compared with those of the $WO_3$/PPy nanocomposites.

## Acknowledgment

This project is financially supported by Research Enhancement Grant (REG) of Lamar University and the National Science Foundation Nanoscale Interdisciplinary Research Team, and Materials Processing and Manufacturing (CMMI 10-30755). D. P. Young acknowledges the support from the National Science Foundation under Grant No. DMR 13-06392. H. Gu acknowledges the support from China Scholarship Council (CSC) program.

## Appendix A. Supplementary data

Supplementary data related to this article can be found at http://dx.doi.org/10.1016/j.polymer.2013.12.024.

## References

[1] Gu H, Huang Y, Zhang X, Wang Q, Zhu J, Shao L, et al. Polymer 2012;53(3):801–9.
[2] Baibich MN, Broto JM, Fert A, Van Dau FN, Petroff F, Etienne P, et al. Phys Rev Lett 1988;61(21):2472–5.
[3] Binasch G, Grünberg P, Saurenbach F, Zinn W. Phys Rev B 1989;39(7):4828–30.
[4] Guo Z, Park S, Hahn HT, Wei S, Moldovan M, Karki AB, et al. Appl Phys Lett 2007;90(5):053111.
[5] Gu H, Zhang X, Wei H, Huang Y, Wei S, Guo Z. Chem Soc Rev 2013;42:5907–43.

[6] Wei H, Yan X, Wu S, Luo Z, Wei S, Guo Z. J Phys Chem C 2012;116(47):25052–64.
[7] Zhang X, Wei S, Haldolaarachchige N, Colorado HA, Luo Z, Young DP, et al. J Phys Chem C 2012;116(29):15731–40.
[8] Gu H, Guo J, Zhang X, He Q, Huang Y, Colorado HA, et al. J Phys Chem C 2013;117(12):6426–36.
[9] Gu H, Guo J, We H, Huang Y, Zhao C, Li Y, et al. Phys Chem Chem Phys 2013:10866–75.
[10] Gu H, Guo J, Sadu R, Huang Y, Haldolaarachchige N, Chen D, et al. Appl Phys Lett 2013;102(21):212403.
[11] Wei H, Yan X, Li Y, Gu H, Wu S, Ding K, et al. J Phys Chem C 2012;116(30):16286–93.
[12] Chiang CK, Fincher Jr CR, Park YW, Heeger AJ, Shirakawa H, Louis EJ, et al. Phys Rev Lett 1977;39(17):1098–101.
[13] Facchetti A. Chem Mater 2010;23(3):733–58.
[14] Gu H, Guo J, He Q, Tadakamalla S, Zhang X, Yan X, et al. Ind Eng Chem Res 2013;52(23):7718–28.
[15] Wang D, Ye Q, Yu B, Zhou F. J Mater Chem 2010;20(33):6910–5.
[16] Wei H, Zhu J, Wu S, Wei S, Guo Z. Polymer 2012;22(33):16817–23.
[17] Kim J, Lee CW, Choi W. Environ Sci Technol 2010;44(17):6849–54.
[18] Vallejos S, Stoycheva T, Umek P, Navio C, Snyders R, Bittencourt C, et al. Chem Commun 2011;47(1):565–7.
[19] Shao Y, Liu J, Wang Y, Lin Y. J Mater Chem 2009;19(1):46–59.
[20] Zhao ZG, Liu ZF, Miyauchi M. Adv Funct Mater 2010;20(23):4162–7.
[21] Gu H, Guo J, Wei S, Guo Z. J Appl Polym Sci 2013;130(4):2238–44.
[22] Zhu J, Wei S, Zhang L, Mao Y, Ryu J, Karki AB, et al. J Mater Chem 2011;21:342–8.
[23] Zhu J, Wei S, Zhang L, Mao Y, Ryu J, Mavinakuli P, et al. J Phys Chem C 2010;114:16335–42.
[24] Gu H, Guo J, Tadakamalla S, Zhang X, He Q, Huang Y, et al. Ind Eng Chem Res 2013;52:7718–28.
[25] Wang J, Khoo E, Lee PS, Ma J. J Phys Chem C 2009;113(22):9655–8.
[26] Gu H, Wei H, Guo J, Haldolaarachchige N, Young DP, Wei S, et al. Polymer 2013;54:5974–85.
[27] Zhu J, Gu H, Luo Z, Haldolaarachige N, Young DP, Wei S, et al. Langmuir 2012;28(27):10246–55.
[28] Guo J, Gu H, Wei H, Zhang Q, Haldolaarachchige N, Li Y, et al. J Phys Chem C 2013;117(19):10191–202.
[29] Guo Z, Shin K, Karki A, Young D, Kaner R, Hahn H. J Nanopart Res 2009;11(6):1441–52.
[30] Aleshin A, Kiebooms R, Menon R, Wudl F, Heeger AJ. Phys Rev B 1997;56:3659–63.
[31] Popok VN, Lukashevich MG, Lukashevich SM, Khaibullin RI, Bazarov VV. Sur Sci 2004;566–568(Part 1):327–31.
[32] Popok V. Rev Adv Mater Sci 2012;30:1–26.
[33] Cruz de la GG, Gurevich YG, Kucherenko V, Arellano de ER. Europhys Lett 2001;53(4):539–43.
[34] Rosenbaum R, Murphy T, Palm E, Hannahs S, Brandt B. Phys Rev B 2001;63(9):094426.
[35] Schoepe W. Z Phys B Condens Matter 1988;71(4):455–63.
[36] Shklovskii BI, Ėfros AL. Electronic properties of doped semiconductors. Springer-Verlag; 1984. p. 3. Appdex.
[37] Gu H, Guo J, He Q, Jiang Y, Huang Y, Haldolaarachchige N, et al. Nanoscale 2014;6:181–9.